EFFECTS OF MORPHOLOGY ON CHARGE TRANSFER PROPERTIES OF ULTRATHIN METALLIC FILMS ON GRAPHITE NANOSTRUCTURES

S. W. Mugo
Jomo Kenyatta University of Agriculture and Technology, Nairobi, Kenya
E-mail: wawerumugo@jkuat.ac.uk

Abstract
The work function on graphitic nanostructures coated with gold, platinum and chromium is reported to be significantly modified by the size and density of the metal nanoparticles. Surface potentials on gold and platinum nanopartides increased to 1.4 V, much higher than that of the bulk metals recorded at 0.45 V and 0.6 V, respectively. On chromium, a sign inversion in the surface potential (SP) was observed with -2 V measured on small nanoparticles and -0.9 V for bulk chromium. The change in sign is shown to result from an inversion in graphite Fermi level, consistent with known doping properties. A relation of the surface potentials with the resulting dipole confirms an occurrence of charge transfer from the metal nanoparticles to the graphitic nanostructure. The charge transfer increased from 0.04 eV to 0.27 eV for nanoparticles ranging between 0.1 nm and 1 nm. These findings demonstrate that besides the choice of metal, morphology of the film can be used to control electronic structure at metal-graphene/graphite interface.

Key words: Nanoparticles, TEM, SAED, SKPM, Surface potential, Charge transfer.

1.0 Introduction

Charge transfer is an important interfacial phenomenon and is useful for graphene/graphite electronics and catalysis on support, (Klusek et al., 2009; Blanter and Martin, 2007; Uchoa et al., 2008; Sutter et al., 2008; Benayad et al., 2009). This occurs when electrons are exchanged between the metal and graphene surface leading to a change in the local density of state (Klusek et al., 2009; Giovannetti et al., 2008). The amount of shift in the Fermi level has been shown to depend on the work function of contacting metal (Uchoa et al., 2008; Benayad et al., 2009; Liu et al., 2011). These studies have been demonstrated using scanning tunnelling microscopy (STM) (Klusek et al., 2009; Li et al., 2009; Brar et al., 2007; Marchini et al., 2007) and photoelectron spectroscopy (Benayad et al., 2009; Pirkle et al., 2009; Obraztsov et al., 2002; Ohgi and Fujita, 2003; Hamada and Otani, 2010). Recent theoretical studies using density function theory (DFT) have further proposed additional interactions from the type of bonding involved (Uchoa et al., 2008; Giovannetti et al., 2008; Hamada and Otani, 2010; Gong et al., 2010; Huard et al., 2008). For physio-adsorbed species, surface electrons delocalize allowing charge transfer, whereas strong chemisorption results in graphite's orbital hybridization (Giovannetti et al., 2008; Liu et al., 2011; Gong et al., 2010). The changing surface electronic structure produces an associated dipole potential (Giovannetti et al.,

2008; Liu et al., 2011; Gong et al., 2010; Gomer, 1975). The crossover in direction of electron transfer, therefore, does not occur when work function difference between metal and graphite is zero, but includes a factor of the interaction distances (Giovannetti et al., 2008; Gong et al., 2010; Jin et al., 2010). The unique doping behaviour of graphite by metals is difficult to explain using existing semiconductor physics (Rusu et al., 2010; Somorjai, 1981). Models so far proposed describe extensively this interaction for uniform monolayer coverage and closest packing possible of metal atoms on graphite surface. However, electronic properties of thin metal films differ from their bulk counterparts (Sun et al., 2010; Gefen et al., 1986). For example, Ohgi and Fujita, (2003) showed that charging produced by Au contacted with molecular layers depend on the amount of conducting electrons and which can be altered by changing the film morphology. Such variation of metal surface atom densities on graphite would produce unique electronic states and chemical reactivities which may not be explained by existing models.

2.0 Experimental procedure

Graphite films from synthetic highly ordered pyrolytic graphite (HOPG) were exfoliated through repeated peeling. Au was then deposited on the graphitic nanostructures through thermal deposition using two different pressures (10-11 and 10-6 mbar). Pt and Cr ultrathin films were also deposited on other samples through sputtering technique. Scanning Kelvin probe microscopy (SKPM) technique both in vacuum and in air was used to obtain surface potentials. Both Au- and Pt-coated tips (ω_0 300 KHz and C = 40 NM^{-1}) were used. To process the results, two independent methods were devised to extract the values: (i) line profiles extending the full scan range and the final value extracted by averaging the SP profiles from all image scans, (ii) raw images were converted to binary images and masked the high contrast regions. This enabled to obstruct the large variations from isolated points and therefore ensured uniform measurements. To check on any ambient effects, the system was vented with air and the measurements repeated. Morphology of the samples was examined with a transmission electron microscope (TEM).

3.0 Results

3.1 Topography and Surface Potential Measurements

Figure 1 shows SKPM scans obtained with Pt tip in vacuum from two samples coated with 1 nm Au at similar conditions. To obtain a representative value, histogram distributions over the whole scan were obtained. Measured potentials are larger than on bulk Au and on fresh graphite surface, as indicated by the arrows. The same position was scanned twice and the process repeated on two other areas of the same sample. The final value was extracted by averaging the mean distributions. To ensure reproducibility, the process was repeated on another sample prepared in similar conditions. Histogram distribution on surface potential scans had a narrow distribution, and with mean value on the nanoparticles larger than on fresh graphite and bulk gold surface.

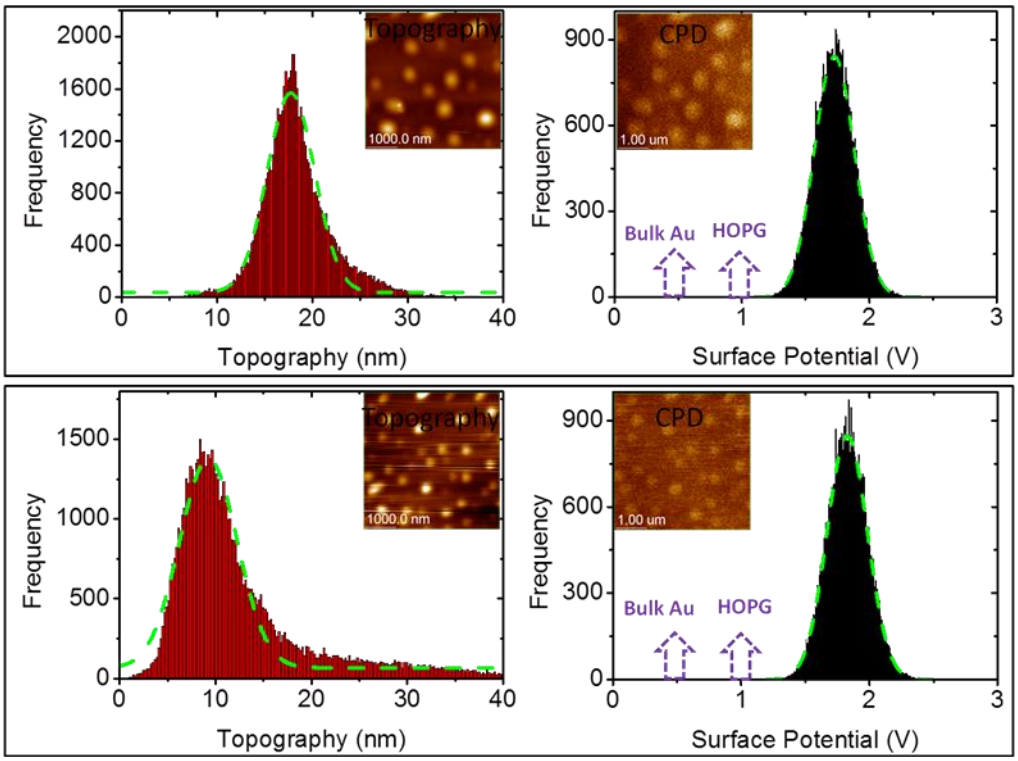

Fig. 1: Histogram distribution on topography and SP on two samples at similar conditions

3.2 Effect of Au nominal thickness

Figure 2 shows SP values on Au coated graphitic films. The data is extracted from histogram distributions, line profiles of raw images and line profiles after masking high contrast region with each data consisting of 8, 16 and 8 values, respectively. Variations given by error bars are smallest after masking high contrast regions attributed to uniform background. The SP curves comprise of: (i) initial increase up to 1.4 V for 1 nm deposition, (ii) exponential decrease with increased Au deposited and (iii) value on thick film. Initial increase is larger than SP on fresh graphite surface and bulk films.

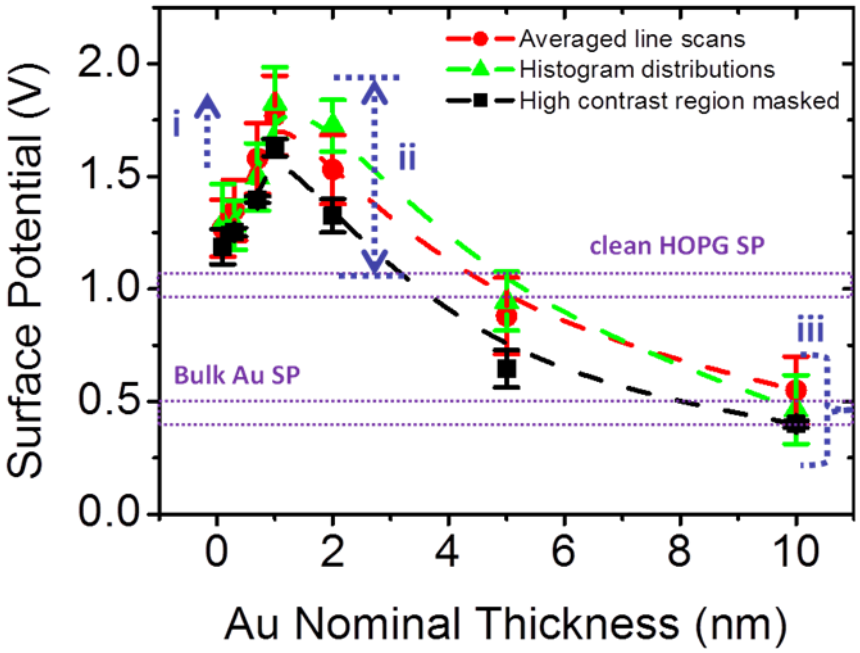

Fig. 2: Surface potential as a function of Au nominal thickness extracted from line averages, histogram distributions and masked high contrast regions.

Comparison with Au films deposited at 10-6 mbar pressure for the same nominal thickness, Fig. 3, shows a good agreement in the overall trends. Values on the thin films are independent of the type of metal tip used, while on thick films the measurements depend on the metal tip. Values of 0.45 V and 0.03 V are measured with Pt and Au tip, respectively.

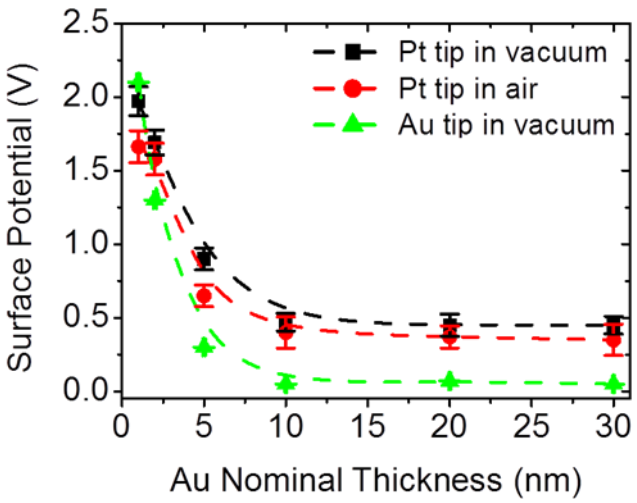

Fig. 3: Surface potentials on Au deposited at 10-6 mbar pressure

Figure 4 displays surface potentials on 1 nm nominal thick Au film after the system was vented with air. Compared to measurements in vacuum, Fig. 2, the values were slightly smaller and with large variations (depicted by error bars), but overall trends were identical.

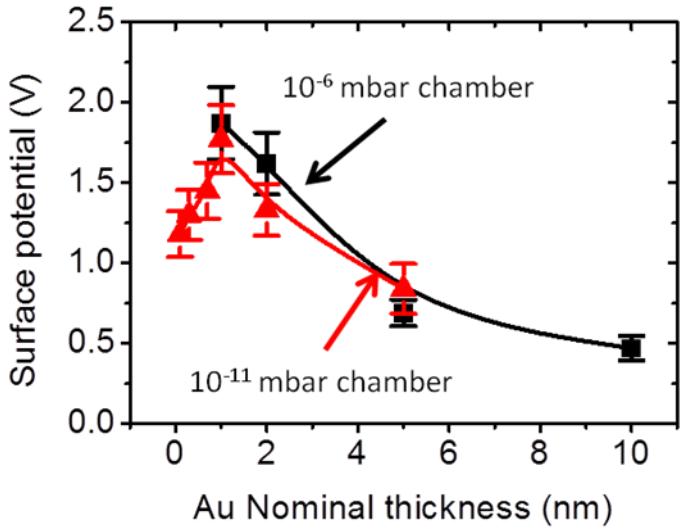

Fig. 4: Surface potentials after venting with air

3.3 Morphology of Au on graphite

Figure 5 shows TEM micrographs of the Au films on graphite. Films initially are discontinuous, consisting of discrete nanoparticles. The particle sizes were determined by approximating spherical geometry and measuring across their diameter. The average separation between nearest neighbours reduced exponentially as particle density increased. Histograms distributions (inset) show small variation in particle widths for films 1 nm. With increased deposition, coalescence dominated with islands eventually linking up to form a continuous film.

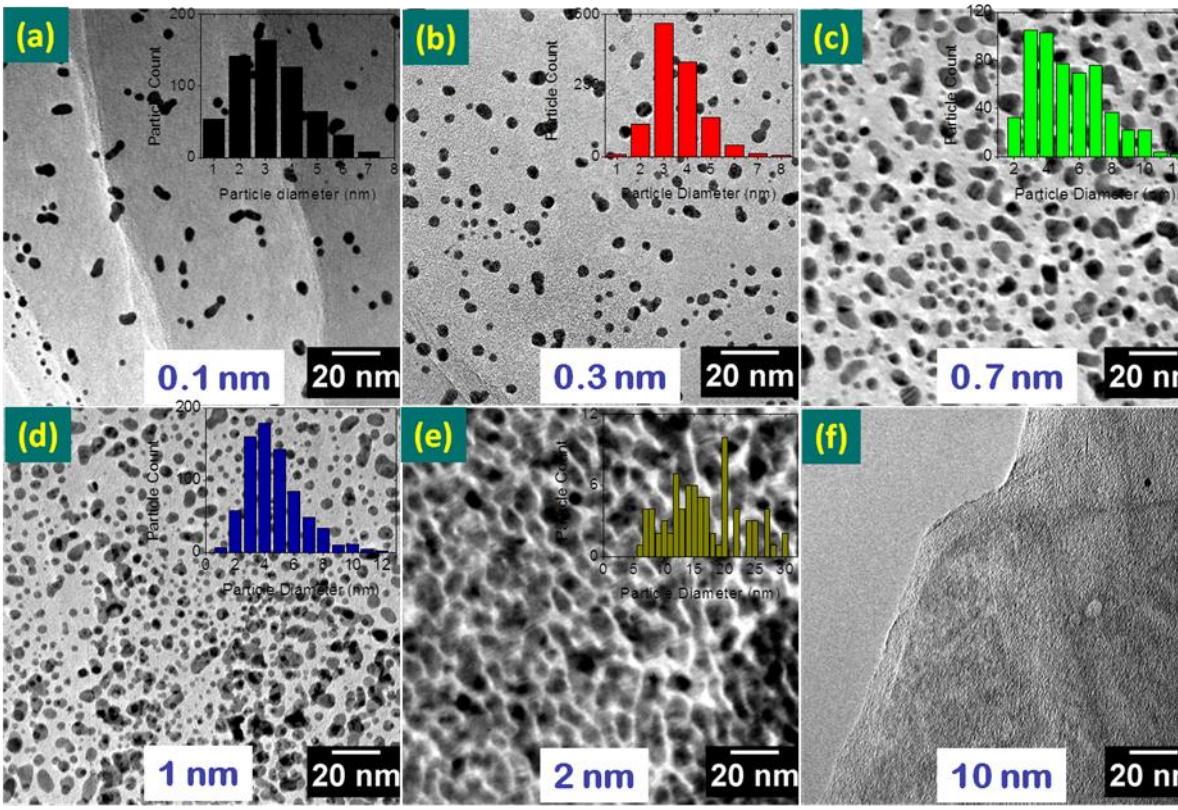

Fig. 5: TEM micrographs of gold on graphite (a) 0.1 nm (b) 0.3 nm (c) 0.7 nm (d) 1 nm (e) 2 nm and (f) 10 nm. (Inset: Histogram distribution of approximated particle widths)

3.4 Effects of contacting Pt and Cr on surface potential

A SP value of 2 V is recorded on 1 nm Pt on graphite nanostructures, with a subsequent exponential decay as shown in Fig. 6a. For film thickness > 10 nm, potentials converged to 0.06 V and 0.5 V as measured with Pt and Au tips, respectively. This trend was very similar to Au deposition. On deposing Cr, a sign inversion was observed with -2 V measured on 1 nm thick (Fig. 6b). For thicknesses > 10 nm SP converged to -0.9 V and -0.65 V as measured with Pt and Au tips, respectively. TEM analysis (Fig. 6 c and d) revealed similar morphologies consisting of discrete nanoparticles. Particle sizes were smaller and of higher density compared to Au of similar deposition. SAED (inset) for both films confirmed the films to be polycrystalline. Although it was not possible to deposit sub-nanometer Pt and Cr films, we see strong correlations with Au: (i) potential increases regardless of metal nanoparticles and AFM tip used, (ii) exponential decrease with metal coverage and (iii) constant value on thick films that depends metal. The trends were also similar after venting the system with air.

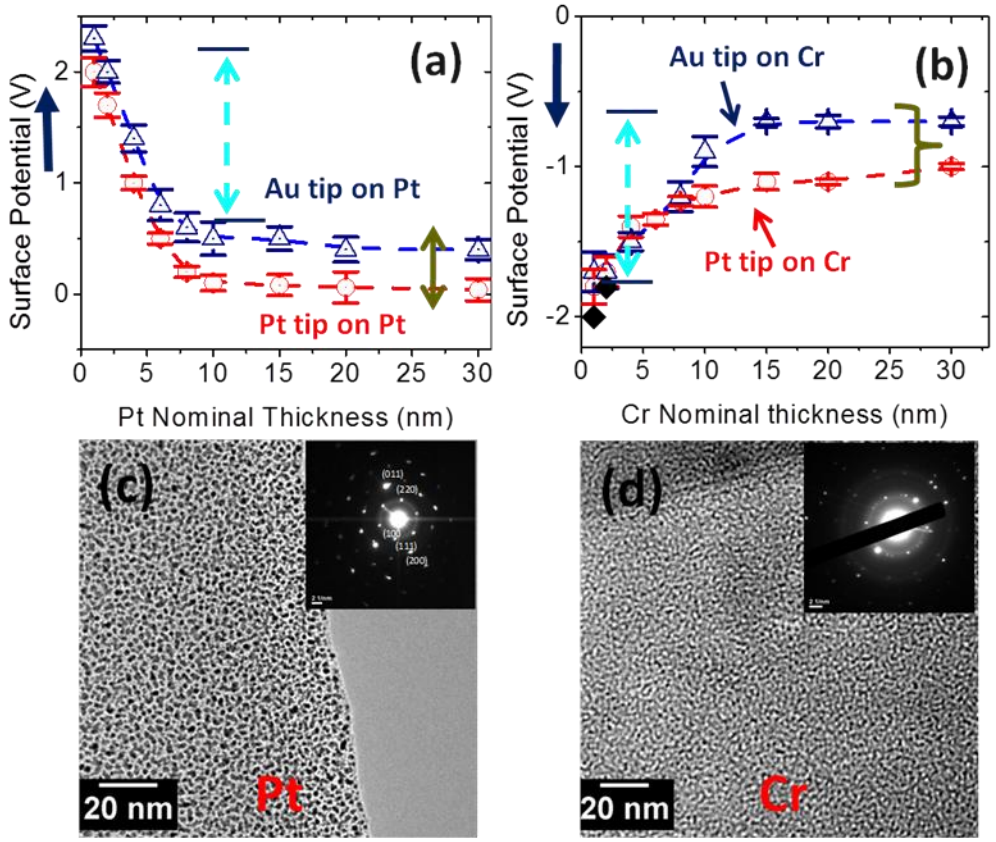

Fig. 6. Surface potential on (a) Pt and (b) Cr, (c) and (d) Corresponding TEM micrographs for 1 nm deposition (inset: SAED pattern).

4.0 Discussion

4.1 Growth of metal films on graphite

The change in film morphology, Fig. 5, is consistent with evolution of thin films (Netterfield and Martin, 1986; Tang, 2003). Initially, atoms arriving on graphite surface have increased kinetics moving around to nucleate with other atoms to form nanoparticles. Electrostatics enhances clusters movement and increased agglomeration. The particle density increases with deposition as several nucleation points are formed, until islands eventually link up to form a continuous film. Figure 7 shows a linear increase in particle density for nominal thickness ⍰ 1 nm. The apparent particle heights from topography scans, Fig. 1, are much larger than real cluster sizes, Fig. 5, due to the large curvature of the AFM tip, causing measured width to broaden.

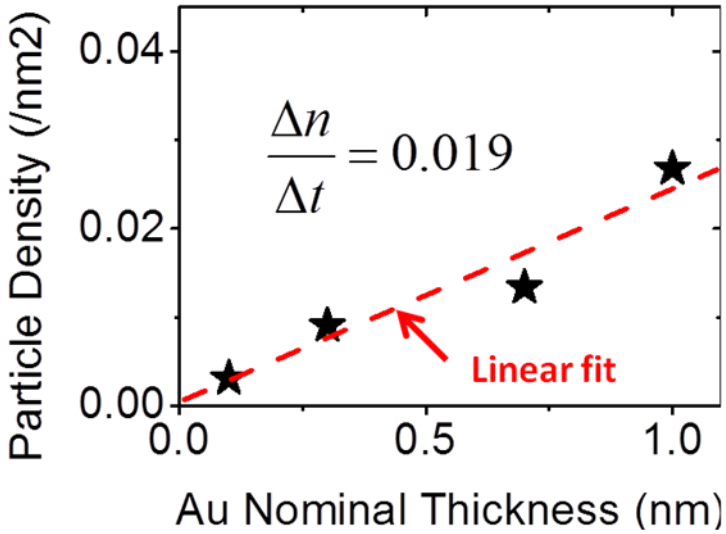

Fig. 7. Variation of particle density with Au nominal thickness

4.2 Electronic structure of metal-graphite interfaces

The 0.97 V and 0.45 V measured on fresh graphite with Pt and Au tips are close to theoretical work function difference of 0.95 V and 0.45 V, respectively. On depositing metals, the initial changes are clearly larger than associated work function consideration (Michaelson, 1978; Michaelson 1950; Sze, 1981). The lack of clear correlation in apparent particle heights from topography with potentials in Fig. 1 is consistent with the argument that topographical heights are largely affected by tip convolution. SP measurements however are an average local value and represent charge distribution on sample (Zerweck et al., 2005; Pandey et al., 2008; Lu et al., 2006). This only affects lateral resolution on individual particles but the spatial resolution is retained. This is confirmed by the fact that SP obtained with different metal tip are identical, indicating changes in sample electronic states whereas values on thick films depend on metal. The large peak-to-peak variations are associated with dipole interactions on selected particles and they only increase error margin, but general trends are retained.

Measured potentials can be modelled to include effects of work function difference ΔV_{WFD}, charge transfer $\Delta V_{transfer}$ and bonding interaction $\Delta V_{bonding}$ between the metal and graphite surface:

$$\Delta V = \Delta_{WFD} + \Delta_{transfer} \quad (1)$$

ΔV_{WFD} and $\Delta V_{bonding}$ are a constant for the same metal. Therefore, the changes would arise from sample charging, expressed as (Giovannetti *et al.*, 2008):

$$\Delta V_{measured} = \frac{e.N}{\varepsilon_0} \quad (2)$$

where *e* is electron charge, *N* is number of electrons transferred per unit area and ε is permittivity of free space. Charging from individual particles can be visualized as dipoles, given by:

$$\Delta V_{measured} = \sum \frac{1}{4\pi\varepsilon_0}(P.n) \quad (3)$$

where *P* is dipole moment from individual particles and *n* is direction normal to field. A plot of the surface potentials with nominal thickness, Fig. 8, shows that SP changes are clearly a function of the average particle density, related by:

$$\Delta V_{measured} = 29.47\Delta n \quad (4)$$

Where Δn is the particle density.

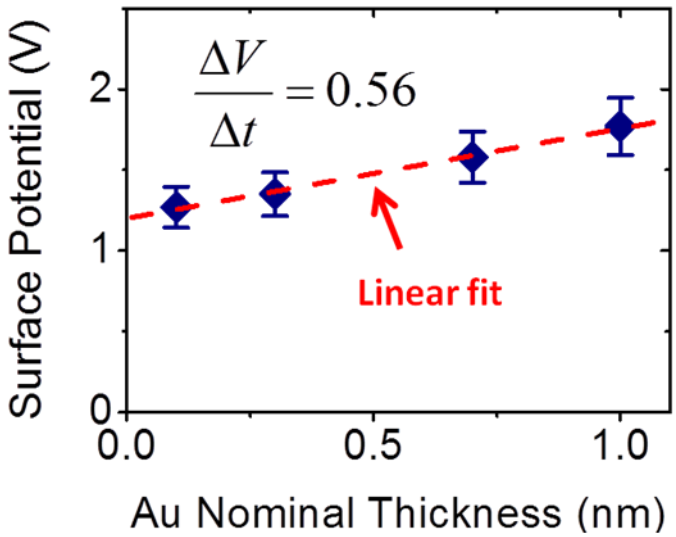

Fig. 8. Variation of surface potential with gold nominal thickness

Since graphite conduct in the c-axis only, the metal tip is influenced by the dipole field beneath it, as illustrated in Fig. 9. However, the cantilever is much larger than the area occupied by a single nanoparticle.

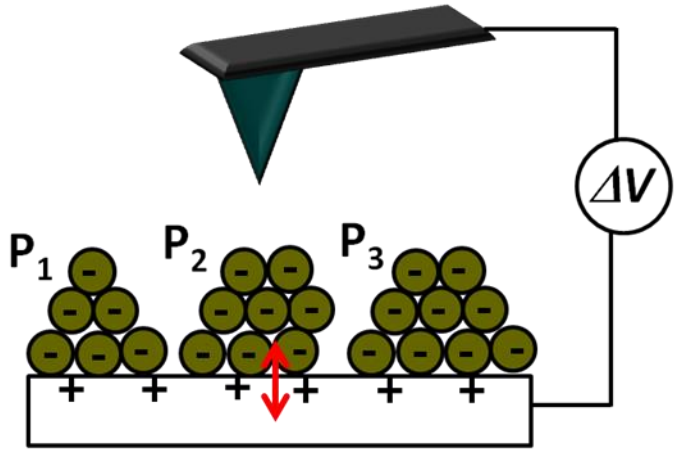

Fig. 9. Schematic illustration of charge symmetry of metal nanoparticles on graphite

The effective field thus originate from the nanoparticles in the vicinity of the tip, resulting in the total dipole being a summation of the dipoles from individual particles, given by eqn. 5.

$$\Delta V_{transfer} = \frac{e.P}{\varepsilon A} \quad (5)$$

By using this relation, we can approximate the charging at Au-graphite interface as displayed in Table 1. This implies that an increase in particle density relates to an increase in the surface atoms available for interaction with graphite surface. This leads to an increased charge transfer. However, these values are much smaller than the computed 1.1 eV for uniform monolayer coverage of Au on graphite by Giovannetti et al., 2008. We attribute this difference to the closest packing of Au atoms. The initial change in sign is consistent with direction of charge transfer as governed by work function of metal (Giovannetti et al., 2008; Liu et al., 2011; Jin et al., 2010). Au and Pt with a higher work function than graphite result in electron flow from graphite to metal. This leaves graphite surface p-doped compared to Cr which has a lower work function than graphite and therefore dopes it negatively.

Table 1: Calculated charging associated with average dipole per nanoparticle

Au Thickness (nm)	$\Delta V_{measured}$ *(V)*	*Dipole moment (D)*	$\Delta V_{transfer}$ *(eV)*
0.1	0.3	0.34	0.04
0.3	0.38	0.54	0.06
0.7	0.61	1.4	0.16
1	0.80	2.41	0.27

Convergence of potentials to a constant value for thick films is attributed to reduced dipole effects as the charged interface is buried below the surface. Thus, electrons in the bulk metal film move within the conduction band. The measured values therefore, result from the interaction of the electrons of the metal film and those of the AFM tip. This corresponds to the work function difference between bulk metal and the metal tip.

5.0 Conclusion

Surface potential measured on graphitic nanostructures contacted with ultrathin films of gold, platinum and chromium has been found to depend on the type of metal and also on the size of nanoparticles. On gold and platinum, the values increased to 1.4 V, much higher than that of the bulk metals recorded at 0.45 V and 0.6 V, respectively. A sign inversion is observed on chromium with -2 V measured for small nanoparticles and -0.9 V for bulk chromium. The change in sign of the work function has been shown to result from an inversion in graphite Fermi level, consistent with known doping properties. Calculation of the resulting surface dipole confirms an occurrence of charge transfer from the metal nanoparticles to the graphitic nanostructure. The charge transfer increased from 0.04 eV to 0.27 eV for nanoparticles deposited within 0.1 nm to 1 nm nominal thicknesses. These results show that besides the choice of metal, morphology can be used to tune the electronic structure on graphite surface. This has great implication in graphene/graphite devices and catalysis on support.

References

Benayad A, Shin H, Park H,Yoon S, Kim K, Jin M, Jeong H, Lee J, Choi J and Lee Y (2009). Controlling work function of reduced graphite oxide with Au-ion concentration. *Chemical Physics Letters,* ***475*** (1-3), 91-95.

Blanter Y and Martin I (2007). Transport through normal metalgraphene contacts. *Physical Review B,* ***76*** (15), 155433.

Brar V, Zhang Y, yayon Y, Ohta T, McChesney J, Bostwick A, Rotenberg E, Horn K and Crommie (2007). Scanning tunneling spectroscopy of inhomogeneous electronic structure in monolayer and bilayer graphene on SiC. *Applied Physics Letters,* ***91***, 122102.

Gefen Y, Shih W, Laibowitz R and Viggiano (1986). Nonlinear behavior near the percolation metal-insulator transition. *Physical review letters,* ***57*** (24), 3097-3100.

Giovannetti G, Khomyakov P, Brocks G, Karpan V, van den Brink J and Kelly P (2008). Doping graphene with metal contacts. *Physical review letters,* ***101*** (2), 26803.

Gomer R (1975). *Interactions on Metal Surfaces.* New York: Springer-Verlag Berlin Heidelberg.

Gong C, Lee G, Shan B, Vogel E, wallace R and Cho K (2010). First-principles study of metalgraphene interfaces. *Journal of Applied Physics,* ***108***, 123711.

Granqvist C and Hunderi O (1978). Selective absorption of solar energy in ultrafine metal particles: Model calculations. *Journal of Applied Physics,* ***50***, 1058.

Hamada I and Otani M (2010). Comparative van der Waals density-functional study of graphene on metal surfaces. *Physical Review B, 82*(15), 153412.

Huard B, Stander N, Sulpizio J and Goldhaber-Gordon D (2008). Evidence of the role of contacts on the observed electron-hole asymmetry in graphene. *Physical Review B,* ***78*** (12), 121402.

Jin K, Choi S S and Jhi S (2010). Crossover in the adsorption properties of alkali metals on graphene. *Physical Review B, 82*(3), 033414.

Kelvin G and Lassabatere (1898). *Philosophy Magazine,* ***46*** (80).

Klusek Z, Dabrowski P, Kowalckyk P, Kozlowski W, Olejniczak W, Blake P, Szybowicz (2009). Graphene on gold: Electron density of states studies by scanning tunneling spectroscopy. *Applied Physics Letters,* ***95*** (11), 113114-113114.

Li G, Luican A and Andrei E (2009). Scanning Tunneling Spectroscopy of Graphene on Graphite. *Physical review letters, 102*, 176804.

Liu H, Liu Y and Zhu D (2011). Chemical doping of graphene. *Journal of Materials Chemistry,* ***21*** (10), 3335.

Lu Y, Munoz M, Steplecaru C, Hao C, Bai M, Garcia N, Schindler K and Esquinazi P (2006). Electrostatic Force Microscopy on Oriented Graphite Surfaces: Coexistence of Insulating and Conducting Behaviors. *Physical Review Letters,* ***97*** (7), 1-4.

Marchini S, Gunther S and Wintterlin J (2007). Scanning tunneling microscopy of graphene on Ru (0001). *Physical Review B, 76*(7), 075429.

Michaelson H (1950). Work Functions of the Elements. *Inorganic Chemistry,* ***536***, 1.

Michaelson H (1978). The work function of the elements and its periodicity. *Journal of Applied Physics,* ***48*** (11), 4729.

Netterfield R and Martin P (1986). Nucleation and growth studies of gold films prepared by evaporation and ion-assisted deposition. *Applied surface science,* ***25***, 265-278.

Obraztsov A, Volkov A, Boronin A and Kosheev S (2002). *Diamond and related materials,* ***11***, 813-818.

Ohgi T and Fujita D (2003). Single electron charging electron effects in gold nanoclusters on alkanedithiol layers with different molecular lengths. *Surface science,* ***532***, 294-299.

Pandey D, Reifenberger R and Piner R (2008). Scanning probe microscopy study of exfoliated oxidized graphene sheets. *Surface Science,* ***602*** (9), 1607-1613.

Pirkle A, Wallace R and Colombo L (2009). In situ studies of Al2O3 and HfO2 dielectrics on graphite. *Applied Physics Letters,* ***95***, 133106.

Rusu P, Giovannetti G, Weijtens C, Coehoorn R and Brocks G (2010). First-principles study of the dipole layer formation at metal-organic interfaces. *Physical Review B,* ***81*** (12), 125403.

Somorjai G (1981). *Introduction to surface chemistry and catalysis.* Canada: Wiley.

Sun Z, Lu J and Song X (2010). Observation of silicon surfaces using ultrahigh vacuum nc-AFM. *Vacuum,* ***85*** (2), 297-301.

Sutter P, Flege J and Sutter E (2008). Epitaxial graphene on ruthenium. *Nature materials,* ***7*** (5), 406-411.

Sze S (1981). *Physics of Semiconductor Devices.* Canada: Wiley.

Tang W (2003). Surface roughness and resistivity of Au substrate. *Microelectronic Engineering, **66*** (1-4), 445-450.

Uchoa B, Lin C and Neto A (2008). Tailoring graphene with metals on top. *Physical Review B, **77*** (3), 035420.

Zerweck U, Loppacher C, Otto T, Grafstrom S and Eng L (2005). Accuracy and resolution limits of Kelvin probe force microscopy. *Physical Review B, **71*** (12), 1-9.